

Article

# Rapid Flood Progress Monitoring in Cropland with NASA SMAP

Md. Shahinoor Rahman, Liping Di \*, Eugene Yu, Li Lin, Chen Zhang and Junmei Tang

Center for Spatial Information Science and Systems, George Mason University, Fairfax, VA 22030, USA; mrahma25@gmu.edu (M.S.R.); gyu@gmu.edu (E.Y.); llin2@gmu.edu (L.L.); czhang11@gmu.edu (C.Z.); jtang8@gmu.edu (J.T.)

\* Correspondence: ldi@gmu.edu; Tel.: +1-703-993-6114

Received: 11 December 2018; Accepted: 17 January 2019; Published: 19 January 2019



**Abstract:** Research in different agricultural sectors, including in crop loss estimation during flood and yield estimation, substantially rely on inundation information. Spaceborne remote sensing has widely been used in the mapping and monitoring of floods. However, the inability of optical remote sensing to cloud penetration and the scarcity of fine temporal resolution SAR data hinder the application of flood mapping in many cases. Soil Moisture Active Passive (SMAP) level 4 products, which are model-driven soil moisture data derived from SMAP observations and are available at 3-h intervals, can offer an intermediate but effective solution. This study maps flood progress in croplands by incorporating SMAP surface soil moisture, soil physical properties, and national floodplain information. Soil moisture above the effective soil porosity is a direct indication of soil saturation. Soil moisture also increases considerably during a flood event. Therefore, this approach took into account three conditions to map the flooded pixels: a minimum of  $0.05 \text{ m}^3 \text{ m}^{-3}$  increment in soil moisture from pre-flood to post-flood condition, soil moisture above the effective soil porosity, and the holding of saturation condition for the 72 consecutive hours. Results indicated that the SMAP-derived maps were able to successfully map most of the flooded areas in the reference maps in the majority of the cases, though with some degree of overestimation (due to the coarse spatial resolution of SMAP). Finally, the inundated croplands are extracted from saturated areas by Spatial Hazard Zone areas (SHFA) of Federal Emergency Management Agency (FEMA) and cropland data layer (CDL). The flood maps extracted from SMAP data are validated with FEMA-declared affected counties as well as with flood maps from other sources.

**Keywords:** flood; soil moisture; SMAP; remote sensing; cropland

## 1. Introduction

Floods are one of the most common, devastating natural hazards around the world considering its scale and impact [1–4]. It is considered the number one natural hazard in the United States (US) [5]. The situation is aggravated by a dramatic increase in flood frequency and intensity due to the recent climate change [6–8]. The agriculture sector is one of the most vulnerable sectors to flooding mainly for two reasons: croplands are outside of the coverage of conventional hazard management systems, and the vast spatial scale of croplands [9]. Almost every year flooding causes significant crop damage over large agriculture area in the US [10–12]. Recent examples are Hurricane Harvey-induced flood, and Hurricane Irma-induced flood in 2017, which accounted for a million-dollar crop loss in the south-eastern parts of the US [13,14]; the Mid-Atlantic river flood in 2012 caused a multimillion-dollar crop loss in the east coast [15]; the Mississippi River flood in 2011 accounted for more than sixty million dollars in the catchment of this river [16]. Therefore, rapid flood progress monitoring is crucial for rapid crop loss assessment, crop condition monitoring, crop insurance, and policy making.

It is challenging to monitor floods over vast agriculture fields using stream gauges. Thus, spaceborne remote sensing has widely been used in flood inundation mapping and monitoring [17,18]. Moderate to coarse spatial resolution optical remote sensing systems (e.g., MODIS, VIIRS, Landsat, Sentinel-2) provide data with fine temporal resolution anywhere from daily to every two weeks. However, optical remote sensing is unable to see through clouds and tree canopies. Therefore, it is difficult to monitor flood progress, especially in the rainy season using optical data due to the possible presence of clouds [18,19]. Moreover, it is difficult to detect storm-induced floods because of the presence of clouds during the low-pressure oceanic condition. Hence, most of the optical remote sensing-based flood monitoring systems are unable to provide flood inundation information during these cloudy conditions. On the other hand, microwave remote sensing brings the opportunity for flood inundation mapping in cloudy condition since microwave systems can penetrate through clouds, aerosol, haze, and tree canopy [18]. Although microwave remote sensing in flood mapping is becoming popular, data from most of the microwave remote sensing systems especially, Synthetic Aperture Radar (SAR), are complicated for processing and are not available free of charge from most of the sources [20]. Free of charge SAR data have recently become available from Sentinel-1 which is a satellite mission of the European Space Agency (ESA). Although the temporal resolution of Sentinel-1 is ideally six days [20], it is very common that SAR data for a particular location may not be available as frequent as Sentinel-1's revisit capability from the official portal of ESA for data download. For instance, Sentinel-1 data are not available to download from the ESA portal for two flood cases (The Texas 2016 Flood and The Mississippi 2016 Flood); however, both flood cases have the duration more than two weeks. Therefore, flood monitoring with SAR data over large agriculture area is not cost effective in many cases. Another challenge is the temporal resolution of these SAR systems, which is more than ten days in most of the cases. Flood lasting less than a week can potentially damage crop depending on the phenology stage of crop. However, flood monitoring with SAR data may fail to detect these short-lived floods. Flood progress monitoring with higher temporal resolution is crucial for many application such as remote sensing based flood crop loss assessment (RF-CLASS) to assess the crop loss from short-lived floods [21–23]. Soil Moisture Active Passive (SMAP), a NASA's satellite mission, launched on January 2015, consisting of L-band microwaves Radar and Radiometer systems. It aims to provide global maps of soil moisture and freeze/thaw state every 2–3 days with high accuracy [24]. One of the key science application of SMAP is to develop improved flood prediction and drought monitoring capabilities [25]. Soil moisture is one of the key components in water-related natural hazards such as a flood. Soil moisture with high temporal resolution can lead to improved flood monitoring and forecasting for medium to vast watersheds where flood frequency and damage is high [25]. Therefore, soil moisture wetness and saturation information from SMAP in combination with ancillary floodplain information can be used to monitor flood [26,27].

Crop condition and growth primarily depend on the balance of two primary resources: soil, water, heat, and nutrients. The soil is the composition of organic matter, minerals, water, and air [28,29]. Any extreme condition such as water shortage or extra water in the soil is detrimental to the crop growth and yield. Plant water stress condition, agriculture drought, takes place when soil moisture goes below the wilting point because there is no water for plant uptake. Similarly, soil moisture at saturation level can significantly damage the crop, since crop roots are unable to adequately respire due to the insufficient oxygen in the soil pores [27,30]. The soil saturation and standing water hamper root growth, leaf area expansion, and photosynthesis. Therefore, this extreme condition, soil saturation, can be called agriculture flood which may lead to damage and crop yield loss. Soil saturation is the condition when all pores between soil particles are filled with water [31]. Fine-textured soil (e.g., clay) usually more porous compared to coarse-textured soils (e.g., sand) [32,33]. Soil moisture content in the volumetric measure is the volumetric water content in soil [33]. The volume of water in soil can vary between zero (dry soil) and the volume of voids between soil particles, which is expressed as the degree of saturation. Volumetric moisture content in a soil equivalent to soil porosity is the indication of fully saturated soil [34–36]. However, some soil pore space may contain entrapped air even when

the soil is considered fully saturated. The percentage of entrapped air is usually between 3% to 7% of void space depending on soil type [33,37]. The total porosity of a soil accounts for both the space available to be filled with water and the entrapped air. Therefore, effective soil porosity for water content can be estimated by 95% (assuming on an average 5% entrapped air) of total soil porosity. Thus, soil moisture content greater than effective soil porosity can be mapped as saturated soil for the indication of agriculture flood.

This study aims to use SMAP surface soil moisture information for the rapid monitoring of flood progress through soil saturation and floodplain information. The usefulness of rapid flood progress monitoring will be evaluated through some case studies on the recent floods in the US. Findings of the study will be helpful for the near real-time flood progress monitoring in cropland to support crop loss estimation, condition monitoring, and immediate policymaking.

## 2. Materials and Methods

### 2.1. Study Area

The current study focuses on five recent floods in the US as case studies. These five cases are chosen from the Federal Emergency Management Agency (FEMA) major disaster declaration (DR). These five cases are Texas Severe Storms and Flooding (DR 4272); Mississippi Severe Storms and Flooding (DR-4268); Louisiana Severe Storms and Flooding (DR-4277); Missouri Severe Storms, Tornadoes, Straight-line Winds, and Flooding (DR-4317); and the Texas Hurricane Harvey Flood (DR-4332) [38]. The Texas Flood event between May 22 and June 24, 2016, impacted more than 20 counties in the Southeastern part of the state. Another flood event struck on March 9, 2016, affecting 17 counties of Mississippi. A month-long severe flood hit more than 24 counties of southern Louisiana on August 11, 2016. The Missouri Flood event flooded more than 30 counties between April 28 and May 11, 2017. The Hurricane Harvey-induced flood from August 23, 2017 to September 15, 2017, affected around 42 counties in the southeastern part of Texas. These five severe flood cases are considered for this study to monitor rapid flood progress using NASA SMAP data.

### 2.2. Data Description

Two datasets are mainly involved with this research: SMAP surface soil moisture and FEMA floodplain (hazard map) information. The SMAP satellite mission consists of both passive (radiometer) and active (SAR) instrument operating in L-band microwave spectrum with multiple polarizations [24]. The goal of the combination of active and passive remote sensing is to achieve the spatial resolution of radar and sensing accuracy of the radiometer. The radiometer measures the emission of the Earth's surface while the active part records backscatter [39]. The SMAP mission has only been providing data from radiometer since July 2015 due to the failure of the active part of the mission [40]. The radiometer instrument on board the SMAP mission observes the L-band (1.4 GHz) microwave radiation emitted from Earth's surface [24,25]. SMAP level 1 (L1) products are the geolocated and calibrated measurements of surface backscatter and brightness temperature [25]. The brightness temperature over the land surface is sensitive to soil moisture of top few centimeters of the soil column [41,42]. Geophysical retrievals of soil moisture products are the level 2(L2) products on a fixed Earth grid based on L1 products and ancillary information [25]. SMAP level 4 (L4) represents the model-driven value-added data products, which provides surface soil moisture, root zone soil moisture, and carbon net ecosystem exchange to support SMAP key applications [24]. The SMAP L4 products are generated using the ensemble-based algorithm assimilating SMAP brightness temperature ( $T_b$ ) observations and the catchment land surface model [42,43]. The reliability of the L4 data, which is validated for many watersheds, is improved due to the utilization of land surface model which relies on conservation principles of water and energy [44]. The spatiotemporal accuracy can further be improved by adding high-resolution radar observations from Sentinel-1 to the SMAP assimilation [45]. SMAP L4 soil moisture data are available every three hours at 9 km spatial resolution [42,44,46]. The latency of

SMAP L4 products is roughly three days because of the primary dependency on the gauge-based precipitation measurement used to drive the land model [47]. The current study utilizes surface soil moisture instead of rootzone soil moisture mainly because surface runoff is more related to surface soil moisture saturation. Moreover, surface soil moisture is a direct measurement in the top five centimeters of soil column, whereas, root zone soil moisture is the estimated value informed by and consistent with surface soil moisture for one-meter soil below the surface. SMAP L4 surface soil moisture data are downloaded from Geospatial Web Service and System [48] for SMAP soil moisture monitoring. Soil moisture data from five-days before the flood event to five-days after the event are considered to cover the whole flood event in each of the five cases. Catchment model soil porosity data of the SMAP soil moisture land model constant dataset is downloaded from the National Snow and Ice Data Center [49]. This study utilized soil porosity for different soil types in the volumetric measure ( $\text{m}^3\text{m}^{-3}$ ) is available at global 9 km EASE-Grid.

Data for the National Flood Hazard Layer (NFHL) of FEMA are collected from the FEMA Flood Map Service Center online archives [50]. This digital database provides flood zone, base flood elevation, and floodway information to support FEMA's National Flood Insurance Program. The demarcated flood zone which is usually the area where most of the flooding occurs. These zones are used by FEMA to designate the Special Flood Hazard Zone (SFHA) and for insurance rating purposes. FEMA defined the SFHA zones which has at least one percent chance of flood in any given year. The one-percent annual chance flood is also referred to as the flood with 100 years return period (base flood). FEMA labeled SFHAs as Zone A, Zone AO, Zone AH, Zones A1-A30, Zone AE, Zone A99, Zone AR, Zone AR/AE, Zone AR/AO, Zone AR/A1-A30, Zone AR/A, Zone V, Zone VE, and Zones V1-V30 [51]. Moderate flood hazard areas, labeled Zone B or Zone X are the areas between the limits of the base flood and flood with 500 years return period (0.2% annual chance). The areas of minimal flood hazard, which are the areas outside the SFHA and at higher than the elevation of the 0.2% annual chance of flood, are labeled as Zone C or Zone X (unshaded). This study uses the SFHA zones (base flood zone) to extract probable inundated areas from soil saturated zones

Cropland Data Layers (CDL) is used to isolate inundated cropland areas to map flood extent in the cropland only. CDL is downloaded from CropScape (<https://nassgeodata.gmu.edu/CropScape/>) for the study area. CropScape is a web service of US Department of Agriculture (USDA) for US geospatial cropland data product [52]. Flood maps derived from SMAP data are validated by comparing them with available flood maps of the selected flood events. Inundation maps of the Baton Rouge Flood are validated by the flood maps available from Stephenson Disaster Management Institute (SDMI) of Louisiana State University. SDMI prepared a flood extent map of the Baton Rouge Flood based on the reported areas that have been flooded. This aggregate flood area then is refined by the LiDAR data to create an elevation appropriate flood area which is published on August 18, 2016 [53]. This may be the only flood map available from authentic source to validate the inundation map of the Baton Rouge Flood extracted from SMAP. Since actual flood maps are not available for other selected flood events, this study uses flood products derived from Sentinel-1 data (SAR-C) for Houston flood and Missouri Flood (Table 1). Sentinel-1 data are collected from the Copernicus open access data hub for each flood event. As long as the microwave can penetrate through clouds, Sentinel-1 data is helpful for accurate flood mapping. Thus, the flood maps derived from Sentinel-1 data are utilized as reference maps for the validation of the flood maps derived from SMAP soil moisture data.

**Table 1.** Summary description of five selected case studies.

Flood Event	DR No. by FEMA	Event Duration	State	No. of Affected Counties	Data Used for Validation
Houston Flood	DR- 4332	August 23–September 15, 2017	Texas	42	Flood map derived from Sentinel-1
Baton Rouge Flood	DR- 4277	August 11–September 10, 2016	Louisiana	24	FEMA-SDMI flood map
May 2017 Missouri Flood	DR- 4317	April 28–May 11, 2017	Missouri	30	Flood map derived from Sentinel-1
March 2016 Mississippi Flood	DR- 4268	March 9–March 28, 2016	Mississippi	17	No data for validation
May 2016 Texas Flood	DR- 4272	May 22–June 24, 2016	Texas	20	No data for validation

### 2.3. Methodology

#### 2.3.1. Flood Mapping from SMAP Surface Soil Moisture

Flooding is associated with the runoff of water after exceeding the highest level of soil saturation level. Soil usually contains lower moisture at dry condition compared to wet condition. Therefore, soil moisture usually increases during saturation. However, some areas such as low lands and wetlands may be always fully saturated. Therefore, soil that is usually dry experiences an increase in moisture for the following inundation except these fully saturated soil throughout the year. After an initial investigation of SMAP level 4 data, this study uses three criteria for flood mapping with SMAP surface soil moisture data. These criteria are a change in the soil moisture content between the flooded condition and non-flooded condition, soil moisture content above the soil effective porosity, and consecutive days of moisture saturation. Figure 1 shows the step by step procedure for cropland flood inundation mapping from SMAP L4 data.

Since the goal of this study is to map inundated areas using soil moisture data, this study observed the soil moisture condition in sampled pixels to verify whether it is possible to detect flood using surface soil moisture from SMAP L4 products. For this purpose, the time series of surface soil moisture are analyzed for sampled pixels extracted from the flooded and non-flooded areas for each case study. Only 70 pixels are sampled from flooded and non-flooded areas for each of the flood cases because of the coarse spatial resolution of SMAP L4 products. The flooded and non-flooded areas in reference flood maps are used as a guideline to select sampled pixels. This process also helps for the estimation of moisture increment threshold. First, soil moisture values are collected over some sampled pixels from both flooded and non-flooded areas for each event. Figure 2 illustrates soil moisture condition in flooded (left panels) and non-flooded pixel (right panels) of five selected flood events. The red lines represent median soil moisture of sampled pixels indicates a significant increase ( $>0.05 \text{ m}^3\text{m}^{-3}$ ) of soil moisture of flooded pixel at the beginning of flood event (light blue shade). Another observation is median soil moisture in flooded pixels cross the  $0.40 \text{ m}^3\text{m}^{-3}$  moisture threshold for most of the sampled location, whereas the median soil moisture of non-flooded pixels remains under the threshold during a flood event. The soil moisture of flooded pixels surpasses the threshold value  $0.40 \text{ m}^3\text{m}^{-3}$ , and returns to previous states at the end of flood events in most of the cases. Some pixels from non-flooded samples have year round high moisture content (Figure 2) probably because of the presence of a higher percentage of saturated soil (e.g., lowlands, wetland) within a pixel [27]. It is hard to distinguish flooded and non-flooded conditions for these pixels based only on the moisture content above the threshold. A considerable change in soil moisture content between pre-flood and post-flood conditions needs to be taken into account for flood mapping with soil moisture data. Since median soil moisture of flooded pixel hovered around  $0.35 \text{ m}^3\text{m}^{-3}$  before the flood and increased to above  $0.4 \text{ m}^3\text{m}^{-3}$  during the flood, a change of  $0.05 \text{ m}^3\text{m}^{-3}$  ( $0.4 \text{ m}^3\text{m}^{-3} \sim 0.35 \text{ m}^3\text{m}^{-3}$ ) in soil moisture can be considered as one of the three indications of flooding.

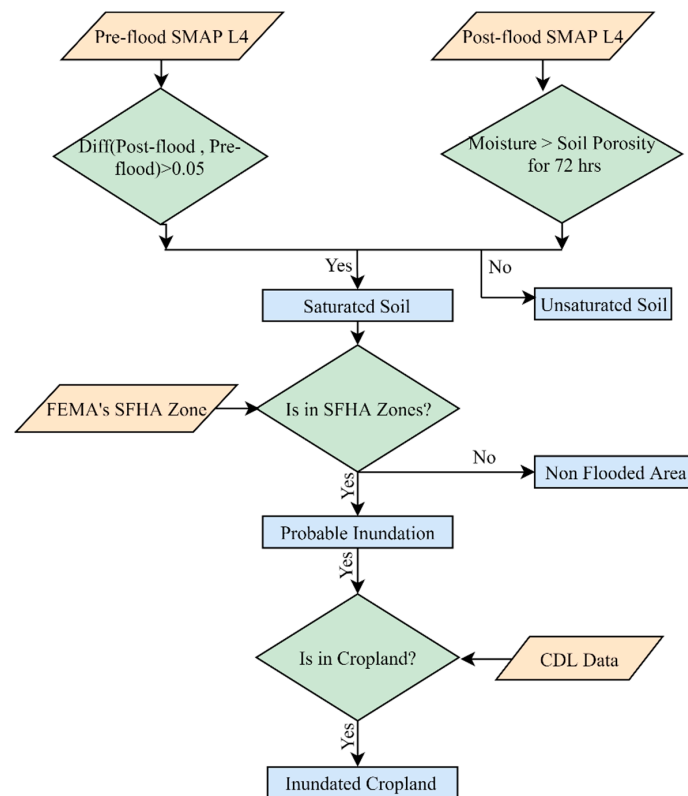
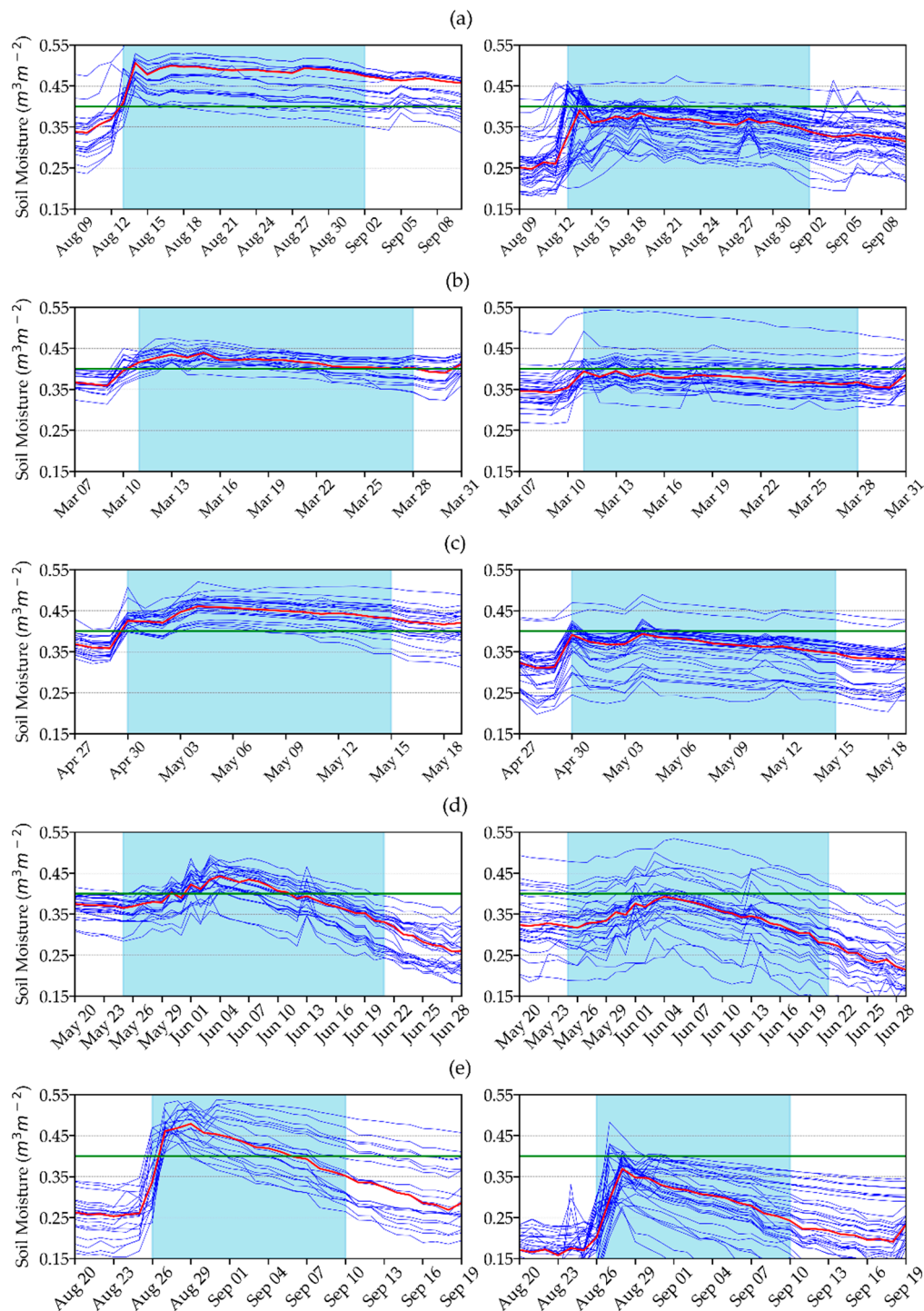


**Figure 1.** Methodological flow diagram for inundation mapping in cropland from SMAP L4 data.

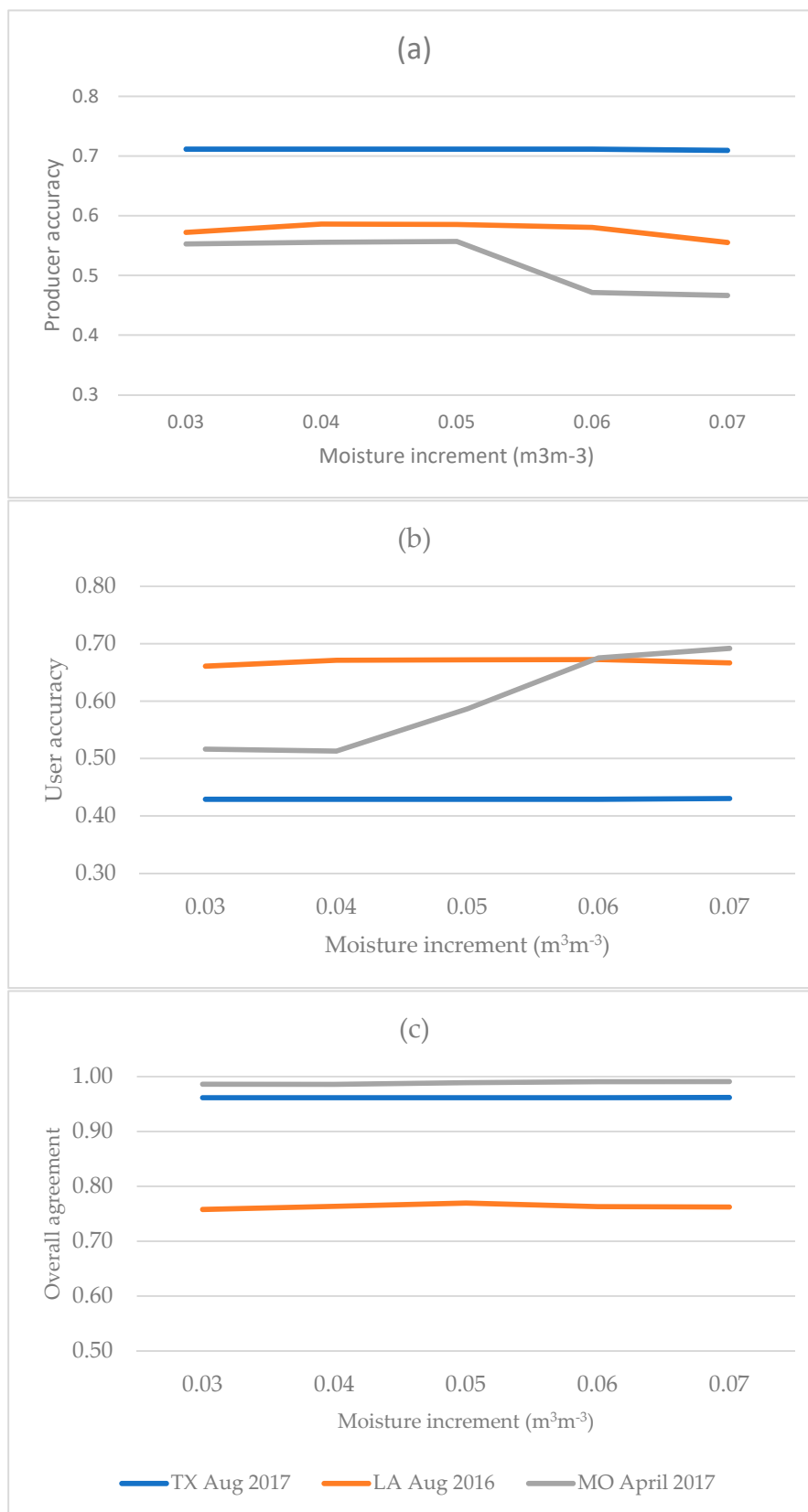
Moisture value above this threshold indicates surface soil moisture saturation, soil moisture increments can be ignored for two reasons: firstly, these random measures can be data noise; secondly, moisture fluctuation within a few hours may not be an indication of flooding. Therefore, observation of soil moisture over a period is essential for flood mapping and monitoring using soil moisture. This study examines with 3-day, 5-day, and 7-day windows as an observation period. Since the windows show similar results, this study applies a 3-day window to observe soil moisture over a consecutive period. Since revisit time of SMAP mission is 2–3 days, an observation window less than three days may not be effective. The sensitivity of soil moisture increment threshold has been tested with different moisture increment values between pre- and post-flood condition from  $0.03 \text{ m}^3\text{m}^{-3}$  to  $0.07 \text{ m}^3\text{m}^{-3}$ . Soil moisture of pre-flood condition is determined by taking the median values of soil moisture in three days before the incident date of the flood event, the whole period of the flooding event is considered as a post-flood condition.

Figure 3 presents the increment thresholds and their accuracy percentages generated by comparing the SMAP-derived flood maps and the reference flood maps across three selected flood events. The spatial agreement is measured using three metrics: overall spatial agreement, user accuracy, and producer accuracy. The overall spatial agreement refers to the proportion of area correctly mapped with the reference map. The producer accuracy is the portion of the reference map correctly mapped; it is the complement of the error of omission. The user accuracy, on the other hand, refers to the proportion of the extracted map that is the same as the reference map; this can also be called the complement of the commission error. The producer accuracy drops when moisture increment threshold is greater than  $0.05 \text{ m}^3\text{m}^{-3}$ . However, the highest producer accuracy is achieved for the increment threshold between  $0.04 \text{ m}^3\text{m}^{-3}$  and  $0.05 \text{ m}^3\text{m}^{-3}$ . The user accuracy also drops or remain unchanged when moisture increment threshold is greater than  $0.05 \text{ m}^3\text{m}^{-3}$  except for the Missouri Flood case. Since flooded areas in most of the case studies show similar moisture increments, the moisture increment threshold is applicable for other flood events as well. The overall spatial agreements between the SMAP-derived flood maps and the reference FEMA flood maps are almost the same for all increment thresholds because of

the dominance of the vast non-flooded areas. Therefore, if a pixel has an increment of  $0.05 \text{ m}^3\text{m}^{-3}$  in soil moisture from pre-flood condition and maintains soil moisture content above the effective soil porosity for three consecutive days (72 h), it is considered as a saturated pixel.



**Figure 2.** Surface soil moisture of sampled pixels over flooded (**left panels**) and non-flooded (**right panels**) pixels; (a) the Louisiana Flood (the Baton Rouge Flood), 2016, (b) the Mississippi Flood, 2016, (c) the Missouri Flood, 2017, (d) the Texas Flood, May 2016, (e) the Hurricane Harvey Flood, TX 2017 (the Houston Flood). Red line indicates the median soil moisture of sampled pixels. Light blue shaded background indicates flood duration.



**Figure 3.** Sensitivity test of moisture increment threshold; (a) producer accuracy, (b) user accuracy, and (c) overall agreement.

There are possibilities of soil saturation on higher slopes or in places where the chance of flood is none. The areas with no or limited chance of flood can be excluded from the flood mapping process. The FEMA's SFHA zones are used as ancillary data to exclude these areas which have no chance of flood. Finally, flood maps are clipped by the CDL data to identify inundated cropland. Flood maps extracted from SMAP L4 data needs to be compared with actual flood map for validation purpose. Since actual flood maps are not available, this study utilized flood maps derived from Sentinel-1 and FEMA-SDMI flood map for validation. Although a strict validation of the results is not possible because of the uncertainties and inaccuracies of the SAR-derived inundation maps and the FEMA-SDMI inundation maps, this study tries to make a relative comparison through the spatial agreement between flood maps derived from SMAP and reference flood maps.

### 2.3.2. Preparation of Reference Flood Map from Sentinel-1 Data

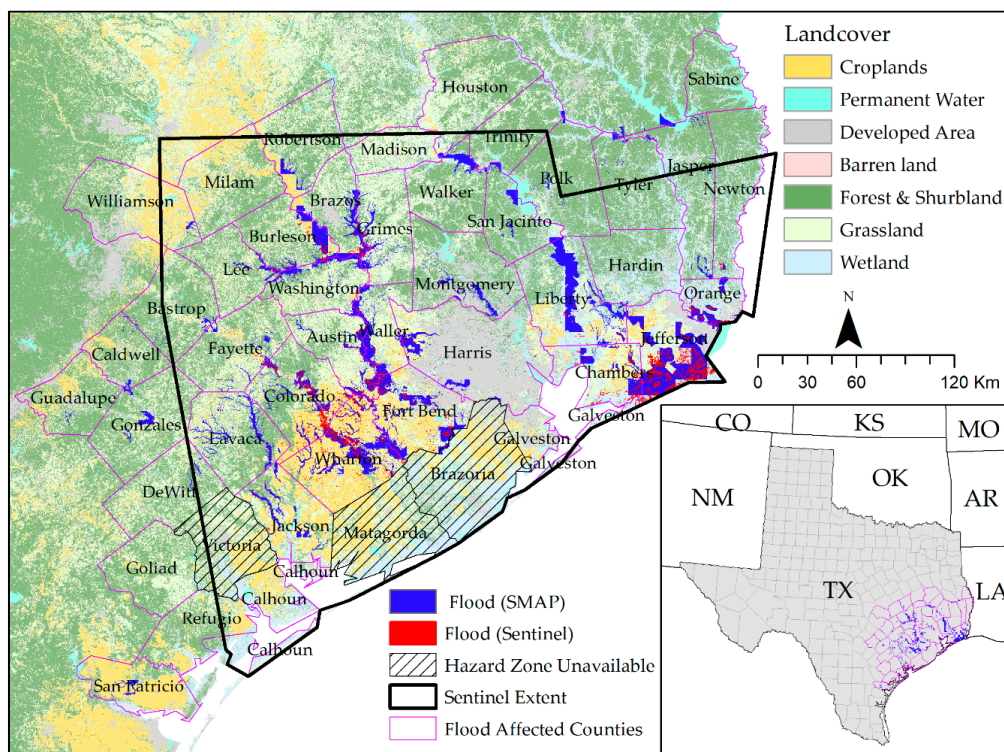
The flood products are derived by analyzing pre- and post-flood Sentinel-1 data for each event. Since the revisit time of Sentinel-1 is more than a week, only a few passes are available within the duration of a flood event. Both pre- and post-flood Sentinel-1 Ground Range Detected (GRD) products are collected for each event from the European Space Agency (ESA) open data hub. Each image has two polarizations: Vertical-Vertical (VV) and Vertical-Horizontal (VH). Images are calibrated using SNAP software (Sentinel toolbox) to calculate sigma naught from available calibration products because sigma naught provides better separation between land and water [54]. Since radar is side looking, Range Doppler Terrain Correction (RDTC) was applied to geocode the images [55]. Finally, the Lee filter with 5 by 5 moving window is applied to reduce the speckle effect of the image. After this pre-processing, log transformation is performed for both pre- and post-flood images of a flood event. Histogram thresholding is used for the binarization (land and water) of the images [56,57]. The cut-off threshold for the histogram varies case by case, roughly around 0.022. Subsequently, a change detection technique is used to extract flood information from pre- and post-flood water information images. SAR-derived flood maps are prone to a number of uncertainties, especially in vegetated areas and urban areas because of the double bounce effect of backscatters [58,59]. SAR backscatter value usually decreases in flooded areas compared to the value in non-flooded conditions. In contrary, backscatter value may increase in emerging flooded vegetation [58]. This study identified open water from Sentinel-1 separately for both pre- and post-flood condition. The change detection is applied between two classified maps instead of the change detection directly on backscatter. Consideration of both increase and decrease in backscatter may improve the flood map extracted from Sentinel-1 [58]. The flood map derived from Sentinel-1 data is used to compare the flood inundation map extracted from SMAP. Since flood inundation maps are available every 3-h, only one inundation map from the same date of available Sentinel-1 data is used for the validation.

## 3. Results

Since this study investigated five flood events as case studies, the findings of this study are presented in separate sections as follow.

### 3.1. Hurricane Harvey Induced Houston Flood in Texas, August 2017

Figure 4 shows the Houston Flood affected areas, extracted from the SMAP and the Sentinel1 data of September 5, 2017. The purple polygons refer to the FEMA-declared affected counties. The thick black line shows the area of which Sentinel-1 data were available. SFHA data were unavailable for these counties marked with black hatch lines, therefore, the figure is not showing any inundated areas in these counties. The figure indicates considerable similarities between extracted flood maps from the SMAP and the Sentinel-1. However, the inundated area from SMAP shows a larger area compared with the inundated area from Sentinel-1 because of the coarse resolution of SMAP data products.



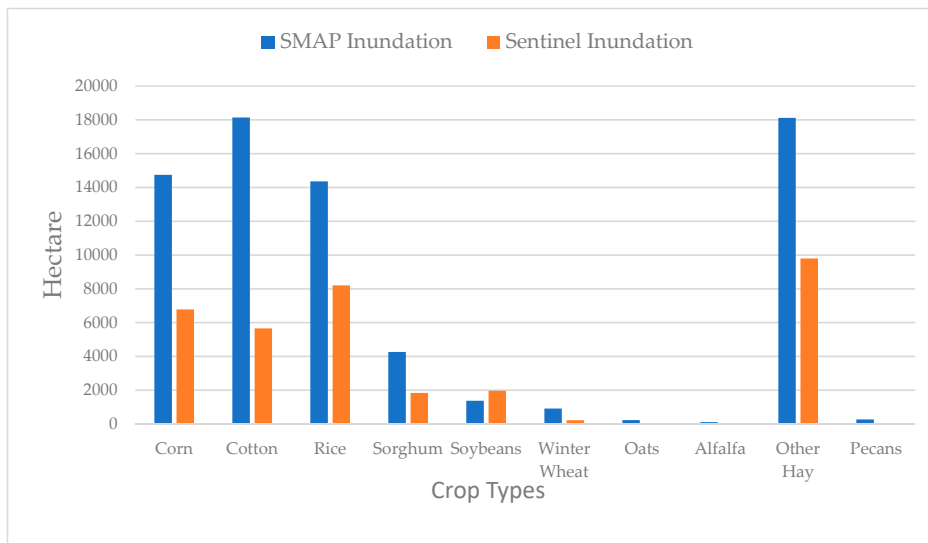
**Figure 4.** Inundation area extracted from SMAP and Sentinel-1 of the Houston Flood superimposed over CDL.

Table 2 shows the spatial agreement between the inundation maps extracted from the SMAP and the Sentinel-1. Although the overall agreement is 96%, the user accuracy and the producer accuracy are 43% and 71%, respectively. The user accuracy of 43% indicates to a commission error nearly 57%, which means that the inundated areas derived from SMAP are almost double than the inundated areas extracted from Sentinel-1 data. The 71% producer accuracy indicates to nearly 30% omission error which means that most of the inundated areas derived from Sentinel-1 are also mapped as inundated areas extracted from SMAP data.

**Table 2.** The spatial agreement between SMAP and Sentinel-1 derived inundation acreage of Houston Flood.

	Non-Flood (Hectare)	Flood (Hectare)	Total (Hectare)	User Accuracy	Errors of Commission
Non-Flood (hectare)	6,062,733	57,930	6,120,663	0.99	0.01
Flood (hectare)	190,228	142,889	333,117	0.43	0.57
Total (hectare)	6,252,961	200,819	6,453,780		
Producer Accuracy	0.97	0.71		Overall	
Errors of Omission	0.03	0.29		Agreement	0.96

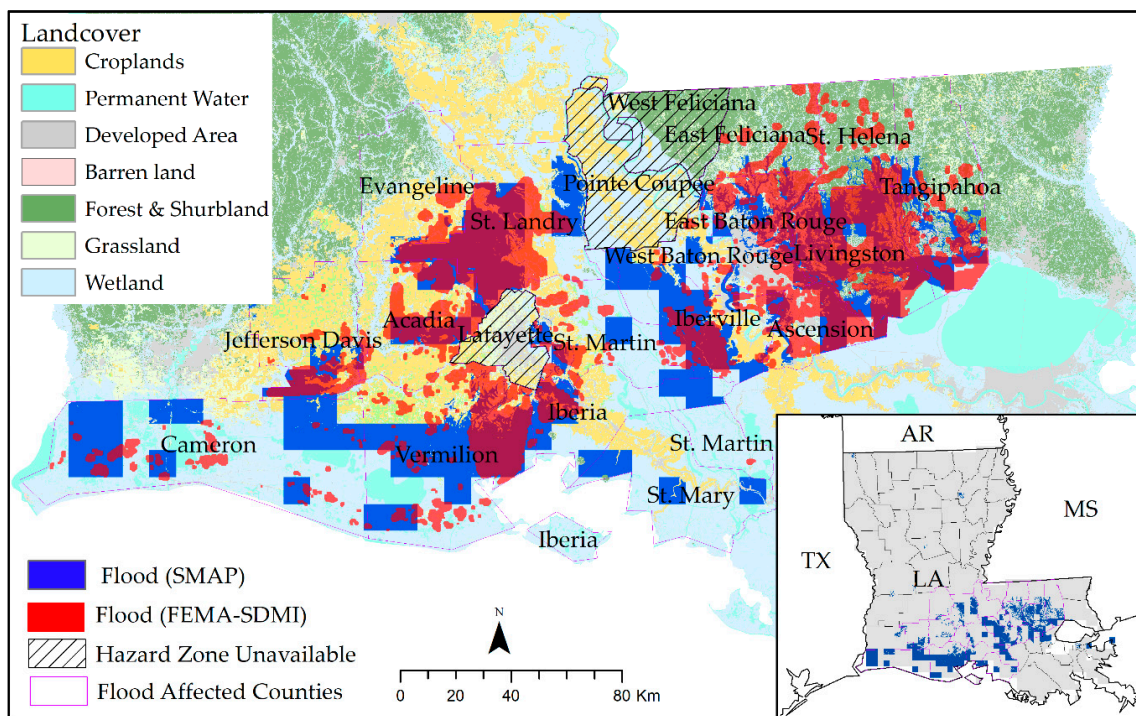
Figure 5 shows the inundated acreage of different crop types in the flood maps derived from SMAP and Sentinel-1. The total inundated acreage of different major crop types shows an overestimation of inundation acreage in SMAP-derived flood map compared to that of the Sentinel-derived one. As observed in the figure, the differences between the SMAP and Sentinel data for crops like soybeans, oats, and pecans, are very small, potentially because these crops are cultivated in fewer croplands. SMAP-derived inundation acreages are almost double than Sentinel-derived inundation acreage for corn and rice. Inundation acreage for cotton is about three times in SMAP-derived flood map than Sentinel-derived flood map. Although this may be an overestimation, SMAP derived inundation information in combination with CDL can help for a very general estimation of crop specific inundation estimation.



**Figure 5.** Comparison of SMAP and Sentinel-1 derived inundation acreage of the Houston Flood over major crop types.

3.2. Baton Rouge Flood in Louisiana, August 2016

Figure 6 compares possible inundation areas extracted from SMAP compared to the flood map obtained from FEMA-SDMI. Although, both the maps have very similar spatial extent, inundated areas are overestimated for some counties like Cameron and Vermilion (Figure 6). The figure also shows some underestimation of flooding for some counties such as Feliciana and St. Helen. This type of underestimation can happen when the spatial extent of the flooded area happens to be significantly smaller than a 9 km SMAP pixel.



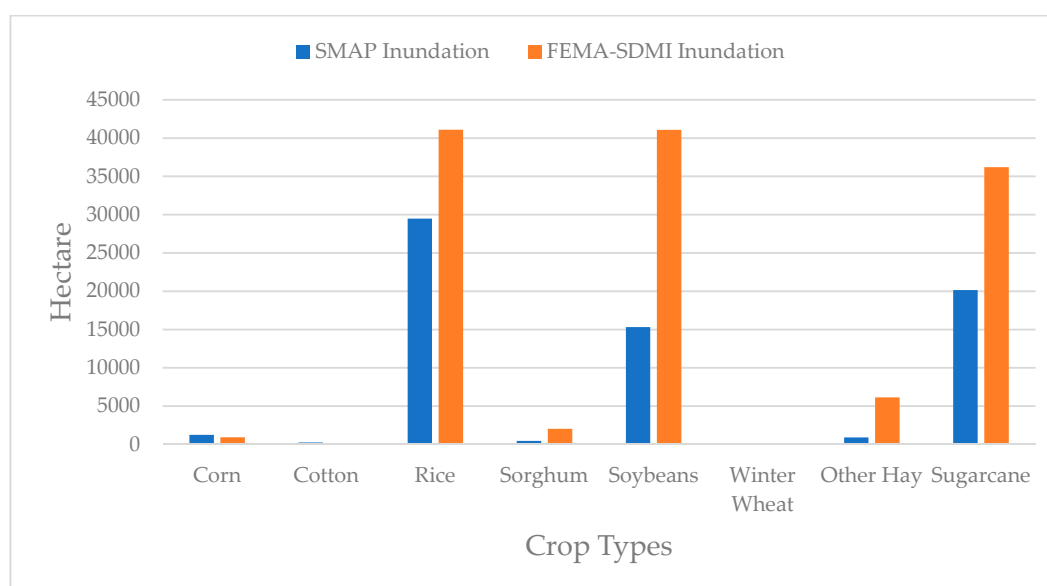
**Figure 6.** Inundation area extracted from SMAP and FEMA-SDMI of the Baton Rough Flood superimposed over CDL.

Table 3 shows the spatial agreement between SMAP-derived flood inundation map and FEMA-SDMI flood map. The overall agreement between the two inundation maps is 77%. The user accuracy of 67% is higher compared to the producer accuracy of 59%. Both omission and commission errors indicate that SMAP-derived inundation map missed nearly 35% of the flooded area and miss-mapped about one-third of non-flooded areas as flooded areas.

**Table 3.** The spatial agreement between SMAP and FEMA-SDMI derived inundation acreage of Baton Rough Flood.

	Non-Flood (Hectare)	Flood (Hectare)	Total (Hectare)	User Accuracy	Errors of Commission
Non-Flood (hectare)	1,742,973	411,934	2,154,907	0.81	0.19
Flood (hectare)	283,956	581,695	865,651	0.67	0.33
Total (hectare)	2,026,929	993,629	3,020,558		
Producer Accuracy	0.86	0.59		Overall Agreement	0.77
Errors of Omission	0.14	0.41			

Figure 7 illustrates a comparative overview of the inundation acreages of the major crops derived from the SMAP and FEMA-SDMI flood maps. As the figure indicates, the inundation acreages are higher in the FEMA-SDMI map than in the SMAP-derived map. The SMAP-derived inundation map shows around 30,000, 15,000 and 20,000 hectares of inundated rice, soybean, and sugarcane, respectively. On the other hand, the acreage of soybeans is more than double in the FEMA-SDMI map than in the SMAP-derived inundation map. This wide range of difference in inundated soybean acreage can be caused, at least, a couple of reasons. First, the FEMA-SDMI map is produced primarily from the reporting of the affected people, which can be prone to errors. And, second, the SMAP uses a coarse spatial resolution, which often can lead to over-estimation due to false-positive results.



**Figure 7.** Comparison of SMAP and FEMA-SDMI derived inundation acreage of the Baton Rough Flood over major crop types.

### 3.3. Missouri Flood May 2017

Figure 8 illustrates the inundation areas of the Missouri Flood extracted from SMAP and Sentinel-1. As it can be observed in the figure, the SMAP derived map is able to capture flood-affected areas in most of the FEMA-declared affected counties. The map derived from Sentinel-1 data also provides similar results. In addition, the spatial extents of flood patches from SMAP are larger than the patches from Sentinel-1. Since hazard zones were unavailable for many counties in Missouri, inundation information was unavailable for these counties. Maps derived from Sentinel-1 indicate that the

spatial location of inundated areas are, in fact, distributed into small and sparse areas. Contrarily, SMAP-derived inundation map captures flood in fewer locations with bigger chunks of areas compared to Sentinel-1-derived flood map.

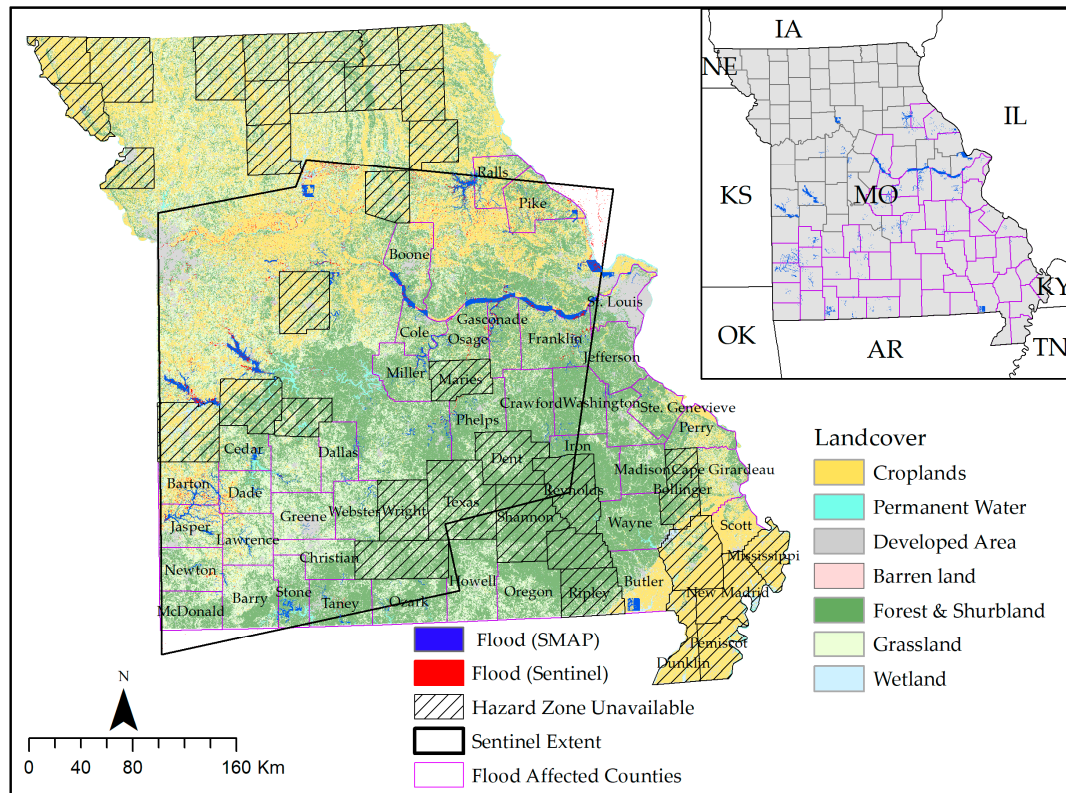


**Figure 8.** Inundation area extracted from SMAP and Sentinel-1 of the Missouri Flood (May 2017) superimposed over CDL.

The user and producer accuracy in the spatial agreement between the SMAP- and Sentinel-1-derived maps are 59% and 51%, respectively (Table 4). The omission error of 51% and the commission errors of 39% indicates to a high disagreement between inundation maps derived from SMAP and the Sentinel-1. A comparison of the inundated acreage of croplands from the two maps is presented in Figure 9. As the figure reveals, the inundated acreage of soybean is three times in the SMAP-derived flood map than the Sentinel-1-derived one. Inundated acreage of corn is almost similar in both maps (about 20,000 hectares).

**Table 4.** The spatial agreement between SMAP and Sentinel-1 derived inundation acreage of the Missouri Flood (May 2017).

	Non-Flood (Hectare)	Flood (Hectare)	Total (Hectare)	User Accuracy	Errors of Commission
Non-Flood (hectare)	7,958,284	52,364	8,010,649	0.99	0.01
Flood (hectare)	37,959	53,832	91,791	0.59	0.41
Total (hectare)	7,996,243	106,196	8,102,439		
Producer Accuracy	1.00	0.51		Overall	0.99
Errors of Omission	0.00	0.49		Agreement	

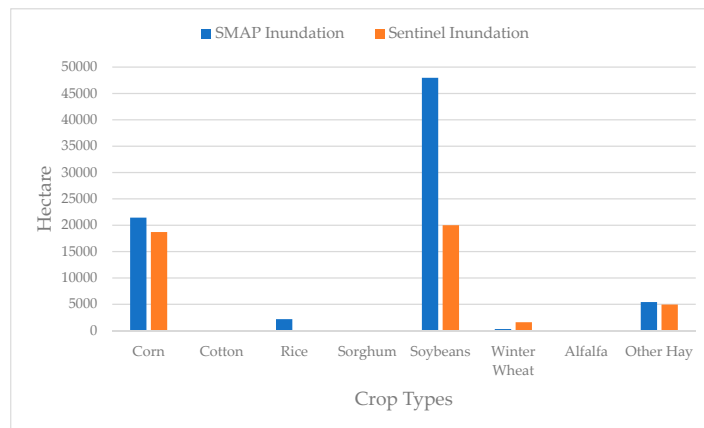


**Figure 9.** Comparison of SMAP and Sentinel-1 derived inundation acreage of the Missouri Flood (May 2017) over major crop types

3.4. Mississippi Severe Storms and Flooding March 2016

Figure 10 shows the inundation maps of the Mississippi Flood 2016, extracted from SMAP. FEMA declared flood-affected counties are shown in purple polygons. Therefore, the figure presents an integrated maps of all inundated areas affected during this flood event. The figure does not show any flood map derived from Sentinel-1 data since they were not available, therefore, no comparison or validation is possible for this flood event. It should be noted that the SMAP-derived map was not able to capture flood in some counties, including Leask, Clarke, and Pearl. This failure to capture some flood areas can, again, happen due to the small spatial extent of the flood on these counties. Figure 11 illustrates the inundation acreages of different major crop types. As the figure indicates, areas with soybean cultivation (nearly 110,000 hectares) were the most affected during the Mississippi Flood, followed by corn, rice, and cotton.

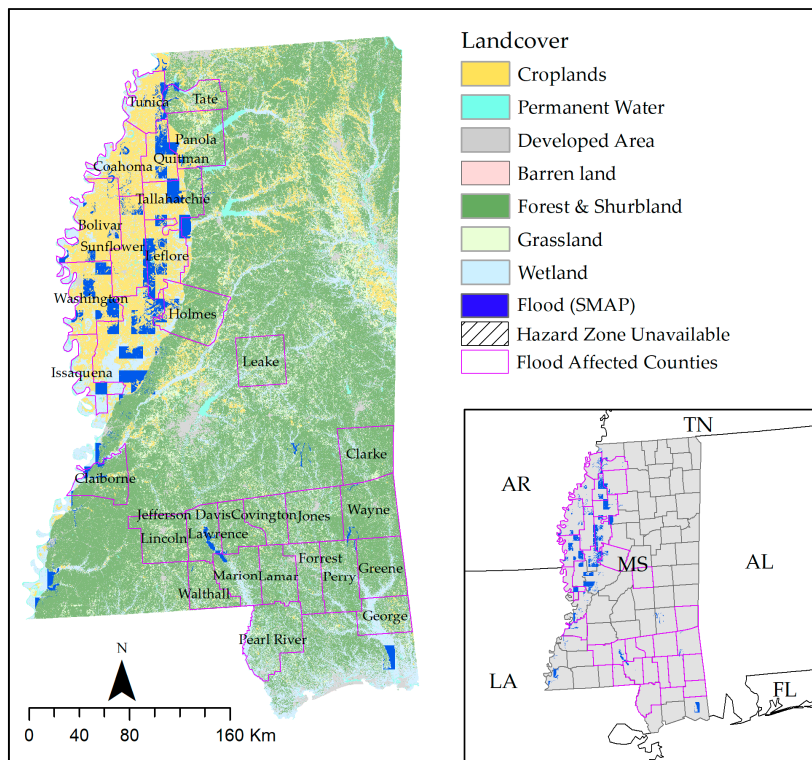


**Figure 10.** Inundation map extracted from SMAP of the Mississippi Flood (March 2016) superimposed over CDL.

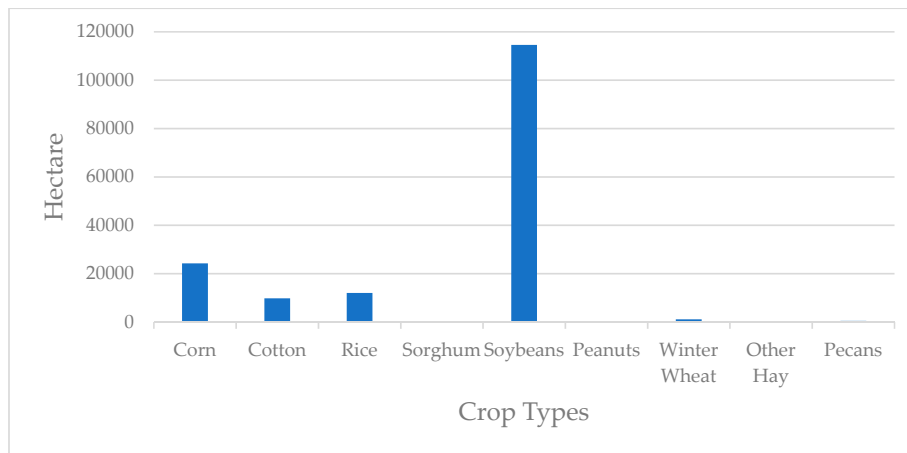


**Figure 11.** Comparison of SMAP derived inundation acreage of the Mississippi Flood (March 2016) over major crop types.

3.5. Texas Flood May 2016

Figure 12 illustrates inundation area during the Texas May Flood extracted from SMAP. Like the Mississippi Flood, Sentinel-1 data were not available for this flood event. Therefore, no comparison or validation of the inundation map is shown here. As the figure indicates, there is large inundated area in the northeastern region outside the FEMA’s declared counties. The inundation acreage of different crop types due to this flood is presented in Figure 13. Corn and cotton, as evident in the figure, are the most affected crops by this flood event, with more than 8000 and 11,000 hectares of areas, respectively.

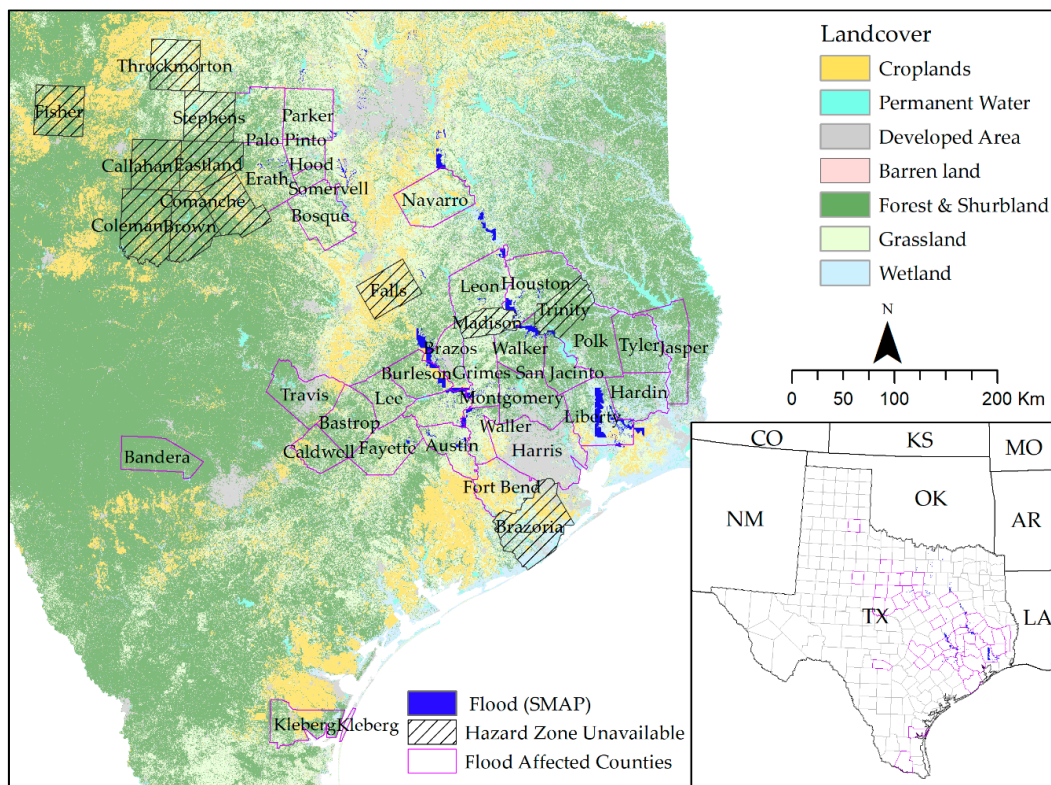


**Figure 12.** Inundation map extracted from SMAP of the Texas Flood (May 2016) superimposed over CDL.

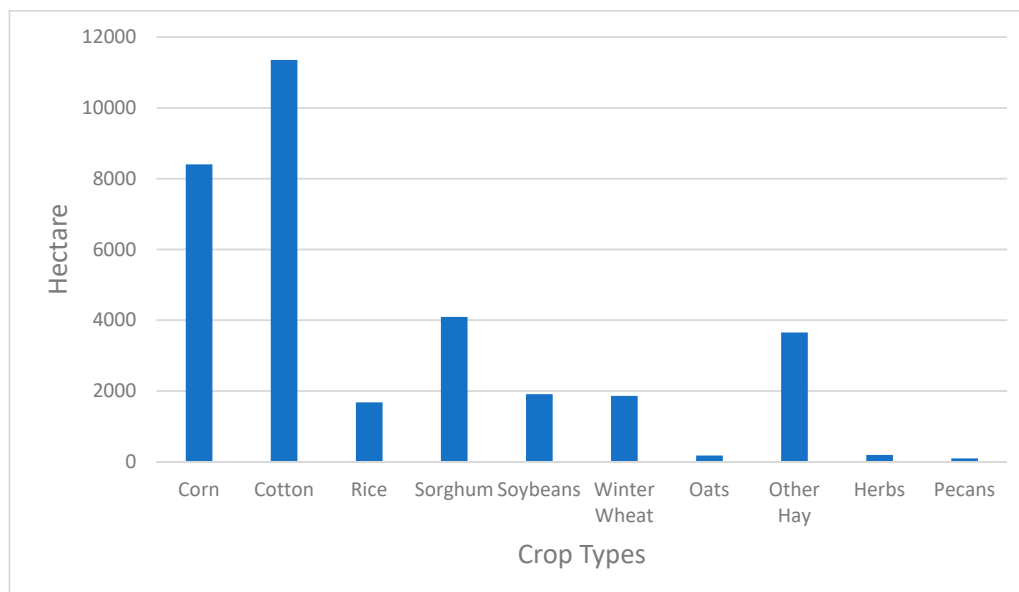


**Figure 13.** Comparison of SMAP derived inundation acreage of the Texas Flood (May 2016) over major crop types.

#### 4. Conclusions

The agriculture sector is one of the most affected sectors by flooding, but the conventional hazard management system pays very limited attention to this sector. Currently, optical remote sensing is widely used for the inundation mapping over a large area. While optical remote sensing systems offer considerable advantages by providing data with remarkably fine spatial resolution and temporal resolution, these systems are incapable for providing data in cloudy conditions. An alternative system is to use the SAR remote sensing because of the cloud penetration capability of microwave. However, coarse temporal resolution and complex data type of SAR systems put limits on more frequent data gathering and processing. Thus, the application of SAR data in flood monitoring for large agriculture regions has not gained much popularity.

This paper evaluates the potential of the use of soil moisture data to overcome the limitations mentioned above. Soil moisture above the effective soil porosity is an indication of soil saturation; and soil saturation in crop field over a longer period of time can be considered as an indicator of cropland inundation. SMAP L4 soil moisture products, which are derived from microwave remote sensing observation (SMAP L1), are available at 3-h intervals, thus it provides much finer temporal resolution than the SAR systems. Therefore, L4 data can provide a useful way to map cropland inundation overcoming the previous limitations. The results in this study provide evidence that inundated areas extracted from SMAP are largely similar to the FEMA's declared counties. Besides, these inundation areas are found to have a similar spatial location with available reference flood maps.

The primary advantage of using the current technique of inundation mapping is that this technique can be used even when the optical or SAR remote sensing data are not available. The relatively small omission error, as reported in this study, indicates that the inundation maps derived from SMAP data were able to map most of the flooded areas in reference maps. Therefore, although the inundation maps are found to overestimate some flooded areas, it is still be useful in generating a rough estimation of inundation area using SMAP soil moisture data.

There are several limitations of using soil moisture data for flood mapping. First, in most of the cases, inundation extents from SMAP are larger than inundation areas derived from the other sources because of the coarse spatial resolution of SMAP. Second, soil moisture data is not available for the paved areas. Therefore, if most of the areas within a pixel contain impervious surface, the resulting soil moisture of the pixel will be low; as a result, it is hard to detect flood for these areas based on the

soil moisture. Future works may focus on SMAP level-1 data which is the direct observation provided by the sensor, instead of the model driven Level-4 surface soil moisture. Despite the limitations, this methodology can be used for cropland inundation mapping even in the absence of fine temporal resolution SAR data. In summary, the inundation map extracted from SMAP soil moisture can be helpful for rapid flood progress monitoring in croplands. The inundation information is also useful for the assessment of crop loss and prediction of future yield; the crop loss estimation and yield estimation can be eventually helpful for policy formulation and decision-making.

**Author Contributions:** M.S.R. and L.D. conceptualized and design the experiment; M.S.R. performed the analysis. E.Y., J.T., L.L. and C.Z. preprocessed preliminary data. M.S.R. wrote the whole article and revised the manuscript. L.D. supervised whole research.

**Funding:** This research was funded by grants from NASA Applied Science Program (Grant # NNX14AP91G, PI: Prof. Liping Di) and NSF INFEWS program (Grant # CNS-1739705, PI: Prof. Liping Di).

**Acknowledgments:** The authors would like to thank, Cropscape portal for the SMAP level4 data achieve and CDL layer and Copernicus for Sentinel open data hub. The authors also would like to express sincere gratitude to FEMA Flood Map Service Center for The National Flood Hazard Layer (NFHL). The authors would also like to thank Stephenson Disaster Management Institute (SDMI) of Louisiana State University for the 2016 Louisiana flood extent map. We would like to thank Md Jahurul Islam of Georgetown University for the proofread of the manuscript. We are also grateful to anonymous reviewers for their valuable comments and suggestions for the improvement of the manuscript.

**Conflicts of Interest:** The authors declare no conflict of interest.

## References

1. Doocy, S.; Daniels, A.; Murray, S.; Kirsch, T.D. The human impact of floods: A historical review of events 1980–2009 and systematic literature review. *PLoS Curr.* **2013**, *5*. [CrossRef]
2. Jonkman, S.N. Global perspectives on loss of human life caused by floods. *Nat. Hazards* **2005**, *34*, 151–175. [CrossRef]
3. Plate, E.J. Flood risk and flood management. *J. Hydrol.* **2002**, *267*, 2–11. [CrossRef]
4. Jonkman, S.N.; Vrijling, J.K. Loss of life due to floods. *J. Flood Risk Manag.* **2008**, *1*, 43–56. [CrossRef]
5. FEMA Flooding: America's #1 Natural Hazard. Available online: <https://www.fema.gov/news-release/2004/08/16/flooding-americas-1-natural-hazard> (accessed on 25 March 2018).
6. Milly, P.C.D.; Wetherald, R.T.; Dunne, K.A.; Delworth, T.L. Increasing risk of great floods in a changing climate. *Nature* **2002**, *415*, 514–517. [CrossRef]
7. Hirabayashi, Y.; Mahendran, R.; Koirala, S.; Konoshima, L.; Yamazaki, D.; Watanabe, S.; Kim, H.; Kanae, S. Global flood risk under climate change. *Nat. Clim. Chang.* **2013**, *3*, 816–821. [CrossRef]
8. Gleick, P.H. Introduction: Studies from the water sector of the national assessment. *JAWRA J. Am. Water Resour. Assoc.* **1999**, *35*, 1297–1300. [CrossRef]
9. Al-Sabhan, W.; Mulligan, M.; Blackburn, G.A. A real-time hydrological model for flood prediction using GIS and the WWW. *Comput. Environ. Urban Syst.* **2003**, *27*, 9–32. [CrossRef]
10. Rosenzweig, C.; Tubiello, F.N.; Goldberg, R.; Mills, E.; Bloomfield, J. Increased crop damage in the US from excess precipitation under climate change. *Glob. Environ. Chang.* **2002**, *12*, 197–202. [CrossRef]
11. Smith, A.B.; Katz, R.W. US billion-dollar weather and climate disasters: Data sources, trends, accuracy and biases. *Nat. Hazards* **2013**, *67*, 387–410. [CrossRef]
12. Downton, M.W.; Miller, J.Z.B.; Pielke Jr, R.A. Reanalysis of US National Weather Service flood loss database. *Nat. Hazards Rev.* **2005**, *6*, 13–22. [CrossRef]
13. Pike, D. The Financial Costs and Consequences of the Escalating Global Warming Emergency. Available online: [http://www.joboneforhumanity.org/the\\_financial\\_costs\\_and\\_consequences\\_of\\_the\\_escalating\\_global\\_warming\\_emergency](http://www.joboneforhumanity.org/the_financial_costs_and_consequences_of_the_escalating_global_warming_emergency) (accessed on 12 April 2018).
14. Quealy, K. The cost of Hurricane Harvey: Only one recent storm comes close. *The New York Times*, 1 September 2017.
15. NOAA National Centers for Environmental Information (NCEI). *Billion-Dollar Weather and Climate Disasters*; NCEI: Asheville, NC, USA, 2018.

16. DeHaan, H.; Stamper, J.; Walters, B. *Mississippi River and Tributaries System 2011 Post-Flood Report*; US Army Corps of Engineers Mississippi Valley Division: Vicksburg, MS, USA, 2012.
17. Sanyal, J.; Lu, X.X. Application of Remote Sensing in Flood Management with Special Reference to Monsoon Asia: A Review. *Nat. Hazards* **2004**, *33*, 283–301. [[CrossRef](#)]
18. Rahman, M.S.; Di, L. The state of the art of spaceborne remote sensing in flood management. *Nat. Hazards* **2017**, *85*, 1223–1248. [[CrossRef](#)]
19. Lin, L.; Di, L.; Yu, E.G.; Kang, L.; Shrestha, R.; Rahman, M.S.; Tang, J.; Deng, M.; Sun, Z.; Zhang, C. A review of remote sensing in flood assessment. In Proceedings of the 2016 Fifth International Conference on Agro-Geoinformatics (Agro-Geoinformatics), Tianjin, China, 18–20 July 2016; pp. 1–4.
20. Grimaldi, S.; Li, Y.; Pauwels, V.R.; Walker, J.P. Remote sensing-derived water extent and level to constrain hydraulic flood forecasting models: Opportunities and challenges. *Surv. Geophys.* **2016**, *37*, 977–1034. [[CrossRef](#)]
21. Di, L.; Eugene, G.Y.; Kang, L.; Shrestha, R.; BAI, Y. RF-CLASS: A remote-sensing-based flood crop loss assessment cyber-service system for supporting crop statistics and insurance decision-making. *J. Integr. Agric.* **2017**, *16*, 408–423. [[CrossRef](#)]
22. Rahman, M.; Di, L.; Yu, E.; Zhang, C.; Mohiuddin, H. In-Season Major Crop-Type Identification for US Cropland from Landsat Images Using Crop-Rotation Pattern and Progressive Data Classification. *Agriculture* **2019**, *9*, 17. [[CrossRef](#)]
23. Shrestha, R.; Di, L.; Eugene, G.Y.; Kang, L.; Li, L.; Rahman, M.S.; Deng, M.; Yang, Z. Regression based corn yield assessment using MODIS based daily NDVI in Iowa state. In Proceedings of the 2016 Fifth International Conference on Agro-Geoinformatics (Agro-Geoinformatics), Tianjin, China, 18–20 July 2016; pp. 1–5.
24. O'Neill, P.; Entekhabi, D.; Njoku, E.; Kellogg, K. The NASA soil moisture active passive (SMAP) mission: OVERVIEW. In Proceedings of the 2010 IEEE International Geoscience and Remote Sensing Symposium (IGARSS), Honolulu, HI, USA, 25–30 July 2010; pp. 3236–3239.
25. Entekhabi, D.; Njoku, E.; O'Neill, P. The Soil Moisture Active and Passive Mission (SMAP): Science and applications. In Proceedings of the 2009 IEEE Radar Conference, Pasadena, CA, USA, 4–8 May 2009; pp. 1–3.
26. Fournier, S.; Reager, J.T.; Lee, T.; Vazquez-Cuervo, J.; David, C.H.; Gierach, M.M. SMAP observes flooding from land to sea: The Texas event of 2015. *Geophys. Res. Lett.* **2016**, *43*. [[CrossRef](#)]
27. Rahman, M.S.; Di, L.; Shrestha, R.; Yu, E.G.; Lin, L.; Zhang, C.; Hu, L.; Tang, J.; Yang, Z.; Zhengwei, D.C. Agriculture Flood Mapping with Soil Moisture Active Passive (SMAP) Data: A Case of 2016 Louisiana Flood. In Proceedings of the 6th International Conference on Agro-Geoinformatics 2017, Fairfax, VA, USA, 7–10 August 2017.
28. Slatyer, R.O. *Plant-Water Relationships*; Academic Press: New York, NY, USA; San Francisco, CA, USA; London, UK, 1967.
29. Denmead, O.T.; Shaw, R.H. Availability of Soil Water to Plants as Affected by Soil Moisture Content and Meteorological Conditions 1. *Agron. J.* **1962**, *54*, 385–390. [[CrossRef](#)]
30. Plant and Soil Sciences eLibrary. Available online: <http://croptechnology.unl.edu/pages/informationmodule.php?idinformationmodule=1130447123&topicorder=2&maxto=13&min=1> (accessed on 17 April 2018).
31. Tapia-Silva, F.-O.; Itzerott, S.; Foerster, S.; Kuhlmann, B.; Kreibich, H. Estimation of flood losses to agricultural crops using remote sensing. *Phys. Chem. Earth Parts A/B/C* **2011**, *36*, 253–265. [[CrossRef](#)]
32. Horn, R.; Taubner, H.; Wuttke, M.; Baumgartl, T. Soil physical properties related to soil structure. *Soil Tillage Res.* **1994**, *30*, 187–216. [[CrossRef](#)]
33. Godwin, R.J. A review of the effect of implement geometry on soil failure and implement forces. *Soil Tillage Res.* **2007**, *97*, 331–340. [[CrossRef](#)]
34. Saxton, K.E.; Rawls, W.J. Soil water characteristic estimates by texture and organic matter for hydrologic solutions. *Soil Sci. Soc. Am. J.* **2006**, *70*, 1569–1578. [[CrossRef](#)]
35. Barker, D.; Beuerlein, J.; Dorrance, A.; Eckert, D.; Easley, B.; Hammond, R.; Lentz, E.; Lipps, P.; Loux, M.; Mullen, R. *Ohio Agronomy Guide*, 14th ed.; Ohio State University Extension: Columbus, OH, USA, 2005; Volume 472.
36. Hudson, B.D. Soil organic matter and available water capacity. *J. Soil Water Conserv.* **1994**, *49*, 189–194.

37. Christiansen, J.E. Effect of entrapped air upon the permeability of soils. *Soil Sci.* **1944**, *58*, 355–366. [[CrossRef](#)]
38. Disasters | FEMA.gov. Available online: <https://www.fema.gov/disasters> (accessed on 18 April 2018).
39. Das, N.N.; Entekhabi, D.; Njoku, E.G.; Shi, J.J.; Johnson, J.T.; Colliander, A. Tests of the SMAP combined radar and radiometer algorithm using airborne field campaign observations and simulated data. *IEEE Trans. Geosci. Remote. Sens.* **2014**, *52*, 2018–2028. [[CrossRef](#)]
40. Chan, S.K.; Bindlish, R.; O'Neill, P.E.; Njoku, E.; Jackson, T.; Colliander, A.; Chen, F.; Burgin, M.; Dunbar, S.; Piepmeier, J. Assessment of the SMAP passive soil moisture product. *IEEE Trans. Geosci. Remote. Sens.* **2016**, *54*, 4994–5007. [[CrossRef](#)]
41. Njoku, E.G.; Entekhabi, D. Passive microwave remote sensing of soil moisture. *J. Hydrol.* **1996**, *184*, 101–129. [[CrossRef](#)]
42. Reichle, R.H.; De Lannoy, G.J.; Liu, Q.; Koster, R.D.; Kimball, J.S.; Crow, W.T.; Ardizzone, J.V.; Chakraborty, P.; Collins, D.W.; Conaty, A.L. Global Assessment of the SMAP Level-4 Surface and Root-Zone Soil Moisture Product Using Assimilation Diagnostics. *J. Hydrometeorol.* **2017**, *18*, 3217–3237. [[CrossRef](#)] [[PubMed](#)]
43. Koster, R.D.; Suarez, M.J.; Ducharne, A.; Stieglitz, M.; Kumar, P. A catchment-based approach to modeling land surface processes in a general circulation model: 1. Model structure. *J. Geophys. Res. Atmos.* **2000**, *105*, 24809–24822. [[CrossRef](#)]
44. Reichle, R.H.; De Lannoy, G.J.; Liu, Q.; Ardizzone, J.V.; Colliander, A.; Conaty, A.; Crow, W.; Jackson, T.J.; Jones, L.A.; Kimball, J.S. Assessment of the SMAP Level-4 surface and root-zone soil moisture product using in situ measurements. *J. Hydrometeorol.* **2017**, *18*, 2621–2645. [[CrossRef](#)]
45. Lievens, H.; Reichle, R.H.; Liu, Q.; De Lannoy, G.J.M.; Dunbar, R.S.; Kim, S.B.; Das, N.N.; Cosh, M.; Walker, J.P.; Wagner, W. Joint Sentinel-1 and SMAP data assimilation to improve soil moisture estimates. *Geophys. Res. Lett.* **2017**, *44*, 6145–6153. [[CrossRef](#)] [[PubMed](#)]
46. Kolassa, J.; Reichle, R.H.; Liu, Q.; Cosh, M.; Bosch, D.D.; Caldwell, T.G.; Colliander, A.; Holifield Collins, C.; Jackson, T.J.; Livingston, S.J. Data assimilation to extract soil moisture information from SMAP observations. *Remote. Sens.* **2017**, *9*, 1179. [[CrossRef](#)]
47. Reichle, R.H.; Liu, Q. *Observation-Corrected Precipitation Estimates in GEOS-5*; National Aeronautics and Space Administration (NASA) Goddard Space Flight Center: Greenbelt, MD, USA, 2014.
48. Hu, L.; Di, L.; Yu, E.; Yue, P.; Tang, J.; Lin, L.; Zhang, C.; Sun, Z.; Hu, R.; Shrestha, R.; et al. Developing geospatial Web service and system for SMAP soil moisture monitoring. In Proceedings of the 2017 6th International Conference on Agro-Geoinformatics, Fairfax, VA, USA, 7–10 August 2017; pp. 1–5.
49. Reichle, R.; De Lannoy, G.; Koster, R.D.; Crow, W.T.; Kimball, J.S.; Liu, Q. *SMAP L4 Global 9 km EASE-Grid Surface and Root Zone Soil Moisture Land Model Constants, Version 4*; NASA National Snow and Ice Data Center Distributed Active Archive Center: Boulder, CO, USA, 2018.
50. FEMA Flood Map Service Center: Search All Products. Available online: <https://msc.fema.gov/portal/advanceSearch#searchresultsanchor> (accessed on 19 April 2018).
51. Flood Zones | FEMA.gov. Available online: <https://www.fema.gov/flood-zones> (accessed on 19 April 2018).
52. Han, W.; Yang, Z.; Di, L.; Mueller, R. CropScape: A Web service based application for exploring and disseminating US conterminous geospatial cropland data products for decision support. *Comput. Electron. Agric.* **2012**, *84*, 111–123. [[CrossRef](#)]
53. SDMI. *Mapping the Extent of Louisiana's Floods*; Stephenson Disaster Management Institute: Baton Rouge, LA, USA, 2016; Available online: <https://www.sdmi.lsu.edu/mapping-the-extent-of-louisianas-floods/> (accessed on 23 May 2018).
54. Bioresita, F.; Puissant, A.; Stumpf, A.; Malet, J.-P. A Method for Automatic and Rapid Mapping of Water Surfaces from Sentinel-1 Imagery. *Remote. Sens.* **2018**, *10*, 217. [[CrossRef](#)]
55. Amitrano, D.; Di Martino, G.; Iodice, A.; Riccio, D.; Ruello, G. Unsupervised Rapid Flood Mapping Using Sentinel-1 GRD SAR Images. *IEEE Trans. Geosci. Remote. Sens.* **2018**, *56*, 3290–3299. [[CrossRef](#)]
56. Psomiadis, E. Flash flood area mapping utilising SENTINEL-1 radar data. In Proceedings of the Earth Resources and Environmental Remote Sensing/GIS Applications VII, International Society for Optics and Photonics, Edinburgh, UK, 27–29 September 2016; Volume 10005, p. 100051G.

57. Step by Step: Recommended Practice Flood Mapping. Available online: <http://www.un-spider.org/advisory-support/recommended-practices/recommended-practice-flood-mapping/step-by-step> (accessed on 10 December 2018).
58. Long, S.; Fatoyinbo, T.E.; Policelli, F. Flood extent mapping for Namibia using change detection and thresholding with SAR. *Environ. Res. Lett.* **2014**, *9*, 035002. [[CrossRef](#)]
59. Tsyganskaya, V.; Martinis, S.; Marzahn, P.; Ludwig, R. SAR-based detection of flooded vegetation—A review of characteristics and approaches. *Int. J. Remote. Sens.* **2018**, *39*, 2255–2293. [[CrossRef](#)]



© 2019 by the authors. Licensee MDPI, Basel, Switzerland. This article is an open access article distributed under the terms and conditions of the Creative Commons Attribution (CC BY) license (<http://creativecommons.org/licenses/by/4.0/>).